

Role of Glycolipids in Lipid Rafts: A View through Atomistic Molecular Dynamics Simulations with Galactosylceramide

Anette Hall

Department of Physics, Tampere University of Technology, P.O. Box 692, FI-33101 Tampere, Finland

Tomasz Róć

Department of Physics, Tampere University of Technology, P.O. Box 692, FI-33101 Tampere, Finland

Mikko Karttunen

Department of Applied Mathematics, The University of Western Ontario, Middlesex College, 1151 Richmond St. N., London (ON), Canada N6A 5B7

Ilpo Vattulainen*

Department of Physics, Tampere University of Technology, P.O. Box 692, FI-33101 Tampere, Finland, Department of Applied Physics, Aalto University School of Science and Engineering, P.O. Box 11100, FI-00076 Aalto, Finland, and MEMPHYS-Center for Biomembrane Physics, University of Southern Denmark, Odense, Denmark

Received: December 25, 2009; Revised Manuscript Received: April 16, 2010

Even in small amounts, glycolipids are an integral part of lipid rafts and their cellular functions. Here we employ atomistic molecular dynamics simulations to consider galactosylceramide (GalCer), one of the common glycosphingolipids, and investigate its interactions with other raft components (cholesterol, POPC, sphingomyelin) as well as the role and the effects of GalCer on the physical properties of raft-like membranes. Our results for 5 mol % GalCer indicate that whereas the thickness of raft membranes is clearly increased by the addition of GalCer, the average area per lipid and lipid conformational order remain virtually unchanged. Notable changes are observed in lateral diffusion of the raft lipids. This is found to be associated with the interdigititation of GalCer. With cholesterol, GalCer is observed to interact specifically by shielding it from the water phase.

1. Introduction

Glycosphingolipids are important components of the outer leaflet of the plasma membranes of most eukaryotic cells. On cell surfaces, they are believed to take part in cell–cell interactions and recognition through glycosignaling domains or glycosynapses.¹ One of the particularly interesting membrane environments where glycosphingolipids are commonly found are lipid rafts, that is, ordered nanoscale cell membrane domains that take part in various dynamic cellular processes such as membrane trafficking, signal transduction, and regulation of membrane proteins.^{2,3}

Together with cholesterol and sphingomyelin, glycosphingolipids are the core constituents of lipid rafts.^{2,4} However, whereas the properties of sphingomyelin and its interactions with cholesterol are rather well understood (see, e.g., ref 5), glycosphingolipids and their interactions with other raft lipids are more challenging to follow. For example, whereas sphingomyelin associates with cholesterol to form domains in the liquid-ordered phase, glycosphingolipids do not readily form cholesterol-enriched domains by themselves. Rather, mixed sphingomyelin- and glycosphingolipid-rich domains appear to incorporate cholesterol.⁶ Meanwhile, although glycosphingolipids, cholesterol, and sphingomyelin are found in ordered membrane domains, their coexistence in the same domain is not estab-

lished.⁷ This is also demonstrated by a recent study that indicated that unlike glycerophospholipids, plasma membrane sphingolipids show transient cholesterol-assisted confinement in domains of <20 nm in size.⁸

In brain tissue, glycosphingolipids comprise up to 10–20 mol % of the lipid constituents in lipid rafts.² Glycosphingolipids are also found in relatively large proportions in, for example, the central and peripheral nervous systems.⁹ In other contexts, the concentration of glycosphingolipids in membranes is usually relatively small. Of common glycosphingolipids, galactosylceramide (GalCer) constitutes ~12 mol % of the white matter in the brain.^{9,10}

The structures of glycosphingolipids are diverse and well-known. They are formed from the basic structure of ceramides, their hydroxyl group being linked to a sugar headgroup. The headgroup can range from simple single carbohydrates such as glucose and galactose to complex oligosaccharide chains with other attached functional groups.¹¹ Ceramides, on the other hand, consist of a long chain of a mostly saturated fatty acid residue linked to a sphingosine base. The domain formation properties of glycosphingolipids are highly dependent on their molecular structure; the size and complexity of the sugar headgroup as well as the length and saturation of the hydrophobic portion are important, in particular, when compared with those of the surrounding phospholipids.⁷ For example, the headgroups of neutral glycosphingolipids with one to two sugar units have been

* To whom correspondence should be addressed. E-mail: Ilpo.Vattulainen@tut.fi

found to be oriented parallel to the bilayer surface.⁷ This functions to allow for tight packing in lipid membranes.

Glycosphingolipids exist in a huge variety of structures, with over 60 ceramide bases and 300 different oligosaccharide chains identified so far.⁴ It is likely that the wide variety of glycolipid headgroups in natural glycolipids is due to their biological function as recognition molecules in plasma membranes.¹² The high melting temperatures and domain formation properties of glycosphingolipids are largely attributed to their ability to form extensive hydrogen bonding networks through their sugar headgroups.¹³ The maximum number of hydrogen bonds that a single cerebroside can form is quite large. For example, in addition to eight acceptor oxygens (each able to form up to two hydrogen bonds), galactosylceramide has six donors in the hydroxyl and amine groups. Compared with other membrane lipids such as sphingomyelin and phosphatidylcholine, the significant fact is the large number of hydrogen bond donors; sphingomyelin has only two donors and phosphatidylcholine does not have any.

The above highlights that whereas the importance of glycosphingolipids in a number of cellular functions is well understood, the role of glycosphingolipids in lipid rafts and especially their molecular interactions with cholesterol and other raft components are only weakly understood. Therefore, atomistic simulations can provide a great deal of added value to complement experiments because they allow one to unravel the mechanisms and the underlying physical principles of molecular processes in atomicistic detail.⁵

Previous work in this context has been very limited. To our knowledge, the first simulations concerned bilayers of lipopolysaccharides,^{14,15} but because of a simulation time scale of ~ 1 ns, the scope of the studied properties was limited. Interactions of gangliosides (GM1) with cholesterol has been recently considered in simulations of ~ 30 ns,¹⁶ focusing on autocorrelation functions of rotational degrees of freedom. More extensive simulations dealt with lipid bilayers including GalCer and dipalmitoylphosphatidylglycerol,¹⁷ the focus being on hydrogen bonding properties at the lipid–water interface. Rög et al.¹⁸ faced the methodological challenges for glycolipids by considering a number of both full-atom and united-atom force fields and validated them against experimental data for phase behavior and lipid packing. Furthermore, Rög et al.¹⁹ considered one-component glycolipid bilayers using headgroups that were based on either the galactose or glucose unit. The study highlighted the complexity of glycolipids because the two cases resulted in substantially different results despite their similarity: glucose and galactose are identical except for their stereochemistry. Findings of similar nature have been made by Chong et al.,²⁰ who found stereochemistry of glycolipids to play a role in the formation of micelles and their structural as well as hydrogen bonding properties. These atomistic simulations highlight the difficulties associated with designing coarse-grained (CG) models for glycolipids because it is a challenge to describe features such as the stereochemistry in CG glycolipid models. This limits the scope of properties that can be studied by CG models for carbohydrates^{21,22} and emphasizes the importance of atomistic simulations for molecular considerations of glycolipid systems.

The aim of this work is to employ atomic-scale molecular dynamics (MD) simulations to study the effects that glycosphingolipids have on the structural and dynamic properties of raft-like membranes. Whereas the structure of lipid rafts has been previously studied computationally,^{5,23–26} the previous simulation models of rafts have overlooked glycosphingolipids, except

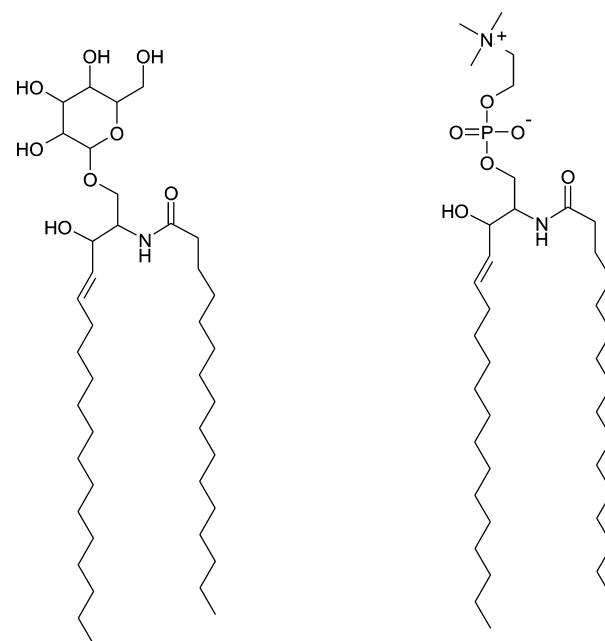


Figure 1. Molecular structures of palmitoyl galactosylceramide (GalCer, left) and palmitoyl sphingomyelin (PSM, right). The stereochemistry is not shown here, but for GalCer, it is that of a normal galactose molecule.

for a study with cholesterol and GM1¹⁶ in the absence of sphingomyelin that is also an integral component of raft membranes. In this study, we take lipid membrane systems similar to those simulated in a previous work on raft systems²³ and add the relatively small amount of ~ 5 mol % of GalCer to establish the effects that galactosylceramides have on the various physical properties of four-component raft-like membranes. Additionally, we study the interactions of GalCer with the other components of membrane rafts. Particular attention is paid to elucidate the interplay of glycosphingolipids with cholesterol as well as sphingomyelin because the favorable interaction of these lipid types seems to be one of the driving forces for raft formation.

2. Model and Analysis

2.1. Model and Simulation Details. In a previous computational study,²³ raft-like membranes were studied through three systems consisting of palmitoyloleoylphosphatidylcholine (POPC), palmitoyl–sphingomyelin (PSM), and cholesterol (CHOL). GalCer was not accounted for in ref 23. In terms of molar concentrations for four-component POPC/CHOL/PSM/GalCer mixtures, the systems considered in ref 23 were 1:1:1:0 (system A), 2:1:1:0 (system B), and 62:1:1:0 (system C).

In this work, similar systems have been enriched with GalCer. (See Figure 1.) We studied three bilayer systems of 256 lipid molecules (128 per monolayer) each. System I contained 82 POPC, 80 PSM, 82 CHOL, and 12 GalCer in addition to 6110 water molecules (POPC/CHOL/PSM/GalCer 1:1:1:0.15). System II contained 120 POPC, 62 PSM, 62 CHOL, and 12 GalCer in addition to 7944 water molecules (POPC/CHOL/PSM/GalCer 2:1:1:0.2). Finally, system III contained 244 POPC and 12 GalCer in addition to 8655 water molecules (POPC/CHOL/PSM/GalCer 1:0:0:0.05).

The structures of GalCer and PSM are closely related. They are both sphingolipids, having a sphingosine base connected through an amide bond to a fatty acid (palmitic acid in this study) to form a ceramide. Ceramide in turn becomes GalCer

with the addition of a galactosyl headgroup or PSM through the addition of a phosphorylcholine headgroup (Figure 1).

The starting coordinates for the bilayers were randomly generated with PACKMOL²⁷ from three molecular configurations of POPC and two molecular configurations of CHOL, GalCer, and PSM. The molecular configurations for CHOL, PSM, and POPC were taken from the previous study,²³ whereas the starting configurations for GalCer were created by combining ceramide parts of PSM with galactose headgroups.^{19,23} After solvation, the energies of all of the initial structures were minimized with the steepest descent algorithm.

The force fields for POPC, PSM, and CHOL were taken from the previous study,²³ except for the double-bond part of POPC, which was slightly modified to better account for its conformational degrees of freedom.^{28–30} We constructed the GalCer force field by combining the ceramide part of the PSM force field with the galactose headgroup part of the force field developed for a galactophospholipid.¹⁹

The simulations were performed using classical atomistic molecular dynamics with the GROMACS software package version 3.3 available from www.gromacs.org.^{31–33} All simulations were conducted in the NpT ensemble with a temperature of 310 K and a semi-isotropic pressure of 1 bar. For the initial equilibration period of 20 ns, we used the weak-coupling thermostat and barostat with respective time constants of 0.1 and 1 ps. After this period, the weak-coupling schemes were replaced with the Nosé–Hoover thermostat and Parrinello–Rahman barostat for the rest of the simulation,^{34–36} using the time constants 0.1 and 1 ps, in respective order. The time step was 2 fs, and the total simulation time for each system was 200 ns. The LINCS algorithm was applied to constrain all of the bonds in the system.³⁷ The van der Waals interactions were calculated up to a cutoff radius of 1 nm. For Coulombic forces, we employed the reaction field (RF) method³⁸ with a truncation distance of 2.0 nm and a dielectric constant of 80. This choice was made based on ref 23, which also used the RF technique. In this manner, our results can be compared with those in ref 23 on equal footing. Recent comparison of the RF method with the particle mesh Ewald (PME) scheme showed that in simulations of lipid bilayers, the RF did not induce artifacts, and the results for RF and PME were essentially identical.³⁹ Additionally, we have simulated a system with a similar composition but 10 mol % of glycolipids for 200 ns using RF and then switched the treatment of electrostatics to PME. The results show that there is no change for the area per lipid of the system (unpublished data), thus validating the use of the RF technique in our case.

2.2. Analysis. The average areas per lipid have been calculated by dividing the total area of a membrane by the number of lipids in a monolayer, and averaging over time after the equilibration period of 20 ns. Bilayer thickness has been calculated from the peak-to-peak distance of the electron density distribution of all atoms in the simulation.

To characterize the dynamics of single tagged lipids, we computed the lateral diffusion coefficient, D , to be

$$D = \lim_{t \rightarrow \infty} \frac{\langle [\mathbf{r}(t + t_0) - \mathbf{r}(t_0)]^2 \rangle}{4t} \quad (1)$$

The coordinates \mathbf{r} are the centers of mass of the molecules, for which the time evolution is examined. In the analysis, the motion of lipids is considered with respect to the motion of the monolayer's center of mass to avoid artifacts due to monolayer motion.^{40,41}

The deuterium order parameters were calculated with the second-order Legendre polynomial

$$S_{CD} = \frac{1}{2} \langle 3 \cos^2 \theta - 1 \rangle \quad (2)$$

from the angles θ of a selected C–H vector and the reference direction, here the bilayer normal. Because hydrogens are not explicitly included in the present united atom model, their positions were reconstructed to the molecules before analysis, assuming ideal positions in given geometries.

We computed the electrostatic potential profile, $\Psi(z)$, by integrating the Poisson equation twice using the boundary conditions $\Psi(0) = 0$ and $E(0) = 0$ for the potential and the electric field, the coordinate along membrane normal, z , being zero in membrane center. Then, one finds⁴²

$$\Psi(z) = -\frac{1}{\epsilon_0} \int_0^z dz' \int_0^{z'} \rho(z'') dz'' \quad (3)$$

where ϵ_0 is the permittivity of vacuum and $\rho(z)$ is the charge density.

Electron density distributions are calculated in the membrane normal direction (z) separately for each molecule type, with the coordinate of the bilayer center set to zero. The electron density profiles for each atom have been calculated in terms of a well-defined electron cloud, which is assumed to be Gaussian distributed around the atom core, using the standard approach in atomistic biomolecular simulations.^{31–33} For comparison between different molecules, the distributions are scaled so that their maximum values are set to one. For consistency, we also computed mass density profiles and found the conclusions for, for example, membrane thickness to be the same.

To study how hydrogen bonding with CHOL molecules affects GalCer headgroup orientation, we investigate the directional vectors of the sugar headgroup for molecules with and without hydrogen bonds to CHOL molecules. The angle distributions are calculated between the bilayer normal and two different vectors. (See Figure 2.) The first one describes the orientation along the sugar headgroup, and its angle with respect to membrane normal is denoted by α . The second vector points in the direction of the normal defined by the plane of the sugar headgroup, and its angle with respect to the bilayer normal is denoted by β . For an ideally oriented GalCer molecule that is standing upright, α should be close to 0°, whereas β should be ~90°.

Existence of hydrogen bonds is judged on geometrical criteria,⁴³ where (a) the distance between donor and acceptor is ≤0.325 nm and (b) the angle between the vector linking donor with acceptor and the vector formed by the chemical donor–hydrogen bond is <35°. The presence of charge pairs⁴⁴ between negatively charged oxygen atoms and positively charged choline methyl groups is based on a cutoff distance of 0.4 nm.

3. Results and Discussion

3.1. Membrane Dimensions. Conformations for the simulated lipid bilayer systems from the simulations are shown in Figure 3, both from the side and from the top of the bilayer. System I is clearly in a liquid-ordered state, with all of the chains neatly arranged, whereas system II is slightly more disordered but still in the liquid-ordered phase. System III is in the liquid-disordered phase, with the chains clearly more randomly arranged. In the top view of system II, one can see a cluster of

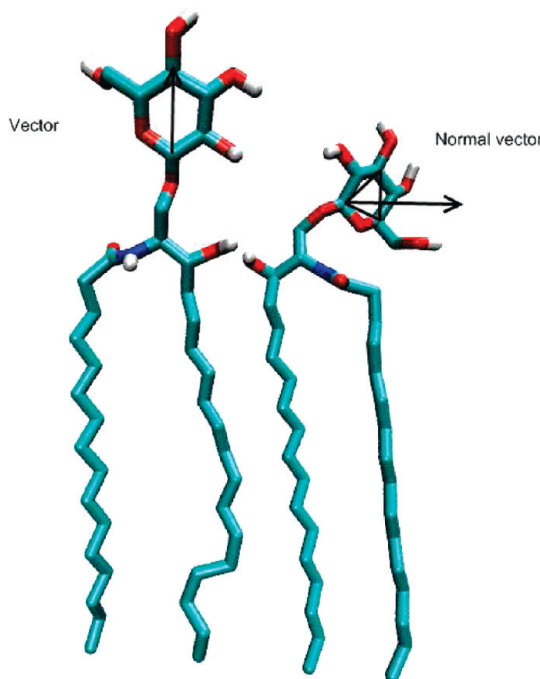


Figure 2. Illustration of the vectors and normal vectors used in the angle distribution calculations.

three GalCer molecules grouped together. This cluster emerged when the system was randomly generated and remained intact throughout the 200 ns simulation, highlighting its stability. The formation of other clusters was not noticed in any of the simulations, which is likely due to the shortness of the simulation time scale. This shows that when formed, such clusters are stable in the sense that their lifetime is large compared with the simulation time scale of 200 ns.

The membrane dimensions, average area per lipid, and bilayer thickness are shown in Table 1. It also depicts a comparison of these results with the previous study by Niemela et al.²³ The error bounds for the area per lipid have been taken from the standard deviation, whereas for bilayer thickness, they have been estimated from the electron density distribution.

The area per lipid is smallest for systems I and A, slightly larger for systems II and B, and >50% larger for systems III and C consisting mostly of POPC. The liquid-disordered systems (systems III and C) exhibit a considerably larger area per lipid because of the less ordered packing of the lipid molecules, whereas the cholesterol-rich liquid-ordered systems are clearly more densely packed. The results are almost identical between the systems containing GalCer and those without (Table 1), indicating that the addition of 5 mol % of GalCer does not change the area per lipid of the different systems.

The bilayer thickness in Table 1 shows that the bilayers that include the largest amount of CHOL (systems I and A) are ~0.1 nm thicker than systems II and B and almost 1.0 nm thicker than the liquid-disordered POPC systems.

Interestingly, the addition of GalCer, while not affecting the area per lipid, noticeably increases the thickness of all of the bilayers. The increase is slight for the liquid-disordered POPC systems and prominent for the systems I and A having ~33 mol % of CHOL. Given that the hydrocarbon region of GalCer is identical to that of PSM and the only structural difference between GalCer and PSM lies in the headgroup region, this substantial change in membrane thickness with no observable change in membrane area is rather surprising. We are not aware of other systems where behavior of this type would emerge.

3.2. Bilayer Profiles. The electron density distributions measured across the bilayer give information on where the atoms or molecular units reside on average in a membrane. For the three studied systems, the normalized electron density distributions for each molecular component are plotted in Figure 4. The first thing one notices about these electron densities is that whereas GalCer has a thickening effect on the bilayer, it is situated below POPC and PSM in all systems. Therefore, the thickening is not caused by GalCer protruding outward from the bilayer but rather it is pushing the phospholipids toward the water phase.

Another interesting property found in the electron densities is that in systems II and III GalCer has a peak in the center of the bilayer, whereas all of the other components have a minimum. In system I, the GalCer electron density dips at the center of the bilayer but less than that of the other lipids. Such a peaking of the electron density at the center of the membrane is caused by interdigitation, ends of the carbohydrate chains extending into the opposite layer.

In a previous study, Niemela et al. found⁴⁵ interdigitation of PSM in one-component lipid bilayers, characterizing the effect of lipid chain length asymmetry. Usually, interdigitation is considered to arise from the asymmetry in lipid chain lengths, and that was precisely what Niemela et al. observed. Meanwhile, when the chain length asymmetry was minor, they found⁴⁵ interdigitation to be rather marginal. In the present case, however, the hydrocarbon chains of GalCer are essentially of identical length, and still GalCer interdigitation is pronounced in systems II and III. We further found that both chains in the glycolipids contributed to interdigitation to a similar degree. It seems apparent that interdigitation is an inherent feature of sphingolipids provided that the opposing leaflet is not exceptionally ordered, blocking the formation of elongated voids that could make interdigitation possible.

Interdigitation in the present systems seems to be governed by the interactions at the membrane–water interface. The GalCer sugar headgroup is seen to be interacting with a phosphatidylcholine headgroup from POPC or PSM via hydrogen bonds and in such a way that the other lipid partly shields the sugar group from water, creating a sort of umbrella over the sugar. At the same time, the sugar group can participate in hydrogen bonds with the other lipids’ carbonyl groups and the hydroxyl of CHOL and POPC. This effect causes the GalCer to be pushed toward the core of the membrane, promoting interdigitation. If one considered single-component bilayers composed of GalCer, then such an effect would not appear because it originates from intermolecular interactions that can only be observed in a mixture of lipids. Snapshots of GalCer interacting in this way can be found in Section 3.8.

The electrostatic potential across the bilayer for each system is plotted in Figure 5. For systems I and II, the electrostatic potential stays negative, and there is a distinct dip before the peaks. In system III, the peak is more pronounced and quite strongly positive.

3.3. Lateral Diffusion. The lateral diffusion coefficients of the lipids are shown in Table 1, again with and without the glycolipid.²³ The lateral diffusion coefficient characterizes the pace of how rapidly the lipids move in the plane of a lipid bilayer in a random-walk-like manner, thus providing insight into the lateral dynamics of lipid mixing. The error bounds for diffusion have been calculated from the standard deviation of the slope of the mean squared displacement.

The overall diffusion coefficients for the liquid-ordered systems (I–II and A,B) with and without GalCer are one order

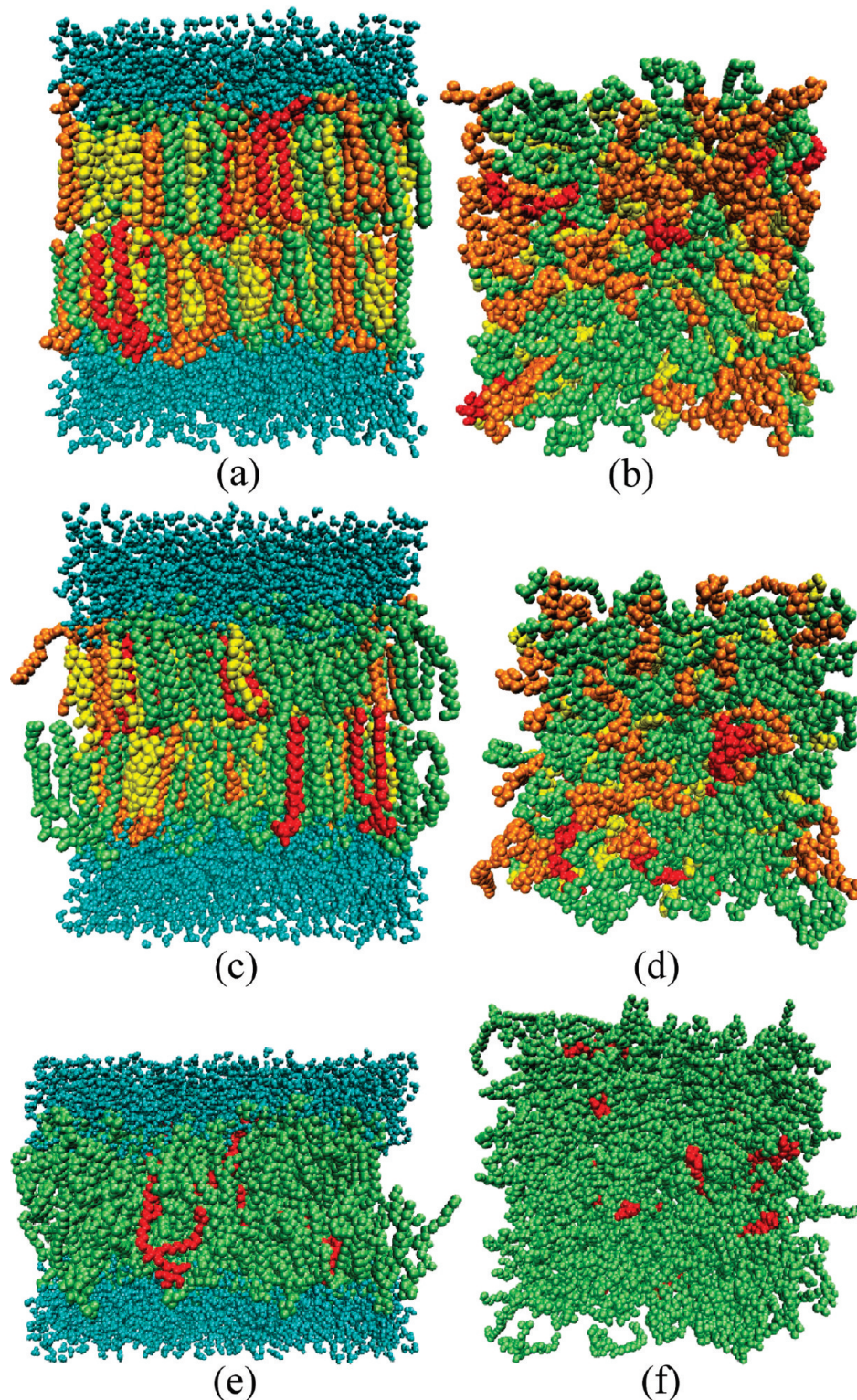


Figure 3. Snapshots from the side and the top of the simulated membranes of the three systems I, II, and III. POPC is green, PSM is orange, CHOL is yellow, and GalCer is red. (a) System I side; (b) system I top; (c) system II side; (d) system II top; (e) system III side; and (f) system III top.

of magnitude smaller than those of the liquid-disordered POPC systems. The difference between the liquid-ordered systems (I vs II and A vs B) is more prominent for the systems without GalCer, with the diffusion of the system B being about double that of the system A.

Another important finding was that the addition of GalCer slows down the average lateral diffusion of the lipids in systems II and III, whereas in system I, there is a slight increase in the

diffusion coefficient. It seems evident that this is due to interdigitation: we find lateral diffusion to slow down for both of the systems (II and III) that exhibited interdigitation but not for the system I where interdigitation is not observed. Similar observations for slowing down of lateral diffusion due to interdigitation has been made in single-component sphingomyelin bilayers,⁴⁵ but in that study, interdigitation was due to asymmetry of lipid chain lengths in PSM molecules. Nonethe-

TABLE 1: Area Per Lipid, Bilayer Thickness, and Lateral Diffusion Coefficients of the Lipids As Averaged over All Lipids in the Systems^a

system	area per lipid (nm ²)	bilayer thickness (nm)	diffusion (10 ⁻⁷ cm ² /s)
system I with GalCer	0.408 ± 0.003	4.56 ± 0.02	0.047 ± 0.003
system II with GalCer	0.445 ± 0.004	4.42 ± 0.02	0.065 ± 0.005
system III with GalCer	0.660 ± 0.008	3.60 ± 0.02	0.55 ± 0.03
system A without GalCer ²³	0.41 ± 0.01	4.40 ± 0.05	0.037 ± 0.002
system B without GalCer ²³	0.44 ± 0.01	4.29 ± 0.05	0.08 ± 0.02
system C without GalCer ²³	0.66 ± 0.01	3.53 ± 0.05	0.7 ± 0.2

^a Results for the present study are compared with those from a previous study by Niemelä et al.²³

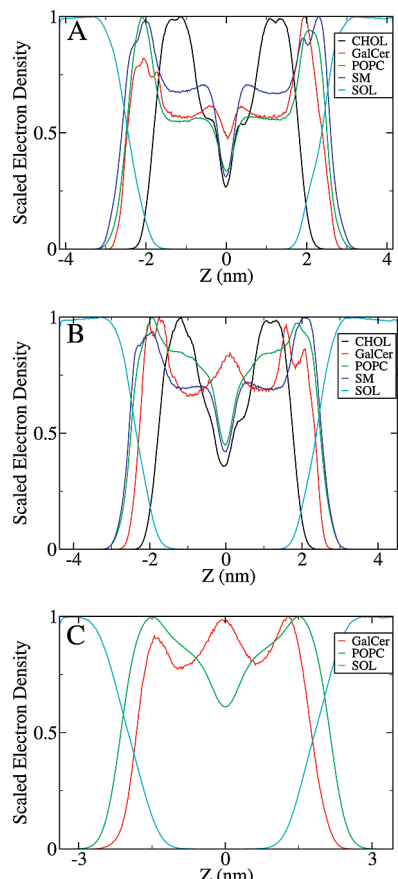


Figure 4. Electron density distributions for the three simulated systems: (A) System I, (B) system II, and (C) system III. The profiles of the two leaflets have not been averaged with respect to membrane center at $z = 0$, and thus the difference of the two leaflets characterizes typical error due to fluctuations in the data. Electron densities have been scaled by the maximum value.

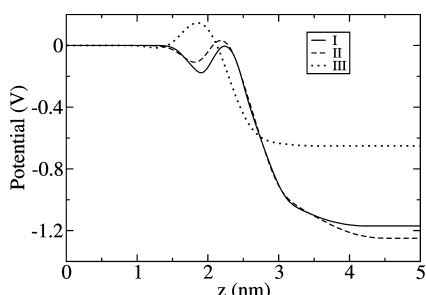


Figure 5. Electrostatic potential across the bilayer for each of the three systems.

less, both the present and the previous findings support the view that strengthening interdigitation and slowing down of lateral diffusion are strongly correlated.

To better understand the effect that the addition of GalCer has on diffusion in the membrane, we consider the diffusion of the individual lipid components. These are shown in Table 2 for all simulations with and without GalCer.

In the systems without GalCer, all three components seem to diffuse at similar speeds in the two liquid-ordered systems. In the systems containing GalCer, the different components exhibit differing diffusion coefficients, the diffusion being the slowest for GalCer and PSM. The diffusion of GalCer is always significantly slower than that of the other lipids. The effect of interdigitation is obvious in this case, too. Furthermore, the presence of GalCer slows down lateral diffusion in the membranes overall, compared with the systems without GalCer.

3.4. Order Parameters. Figure 6 shows the order parameters for each of the different carbon chains for the three systems. We find that system II is slightly less ordered than system I, whereas system III is clearly more disordered than the others. The ordering of the POPC *sn*-2 chain notably differs from the others because of the double bond in this chain. In system I, the ordering of the PSM and GalCer chains is remarkably similar, with the exception of the GalCer acyl-chain becoming less ordered toward the end of the chain. GalCer is somewhat less ordered in system II than the other components. In the first two systems, the sphingosine-chain in PSM is the most ordered.

Previously the ordering of the carbon chains in a system without GalCer has been studied through the average order parameter of carbons 5–7 for all components.⁴⁶ The obtained results were: 0.41 for the system corresponding to system I, 0.36 for the system corresponding to system II, and 0.18 for the system corresponding to system III. For the systems containing GalCer, these values are identical, indicating that there is no real change in the ordering of the hydrocarbon chains caused by the addition of GalCer.

3.5. Radial Distributions. Radial distributions of the different lipid types around CHOL molecules are shown in Figure 7 for systems I and II. The RDF $g(r)$ describes the average distribution of centers of mass of lipid components around others as a function of distance. The results obtained in this work are well in line with those calculated in the previous study without GalCer.²³ The CHOL–CHOL distribution in Figure 7A has a very distinct peaked behavior, whereas the distribution of POPC around CHOL molecules in Figure 7B is slightly peaked only at short distances, quickly settling to an even distribution. The CHOL–PSM and CHOL–GalCer distributions are quite similar to each other and clearly different from that of CHOL–POPC.

The distributions of POPC and PSM molecules around GalCer molecules are presented in Figure 8. It is interesting that in the GalCer–PSM distribution, GalCer has more neighbor peaks in system I than in system II. Also, the GalCer–PSM and CHOL–GalCer (Figure 7D) distributions are surprisingly similar, possibly indicating that these three are somehow organized in the systems. The GalCer–POPC distribution in Figure 8B shows that in system II the pair correlation is almost

TABLE 2: Lateral Diffusion Coefficients for Each Lipid in the Simulated Systems Compared with Ones from a Previous Study by Niemelä et al.²³

lateral diffusion [10 ⁻⁷ cm ² /s]	D _{GalCer}	D _{CHOL}	D _{POPC}	D _{PSM}
system I with GalCer	0.025 ± 0.004	0.053 ± 0.004	0.056 ± 0.004	0.035 ± 0.004
system II with GalCer	0.046 ± 0.008	0.07 ± 0.02	0.070 ± 0.005	0.057 ± 0.004
system III with GalCer	0.34 ± 0.08		0.56 ± 0.03	
system A without GalCer ²³		0.038 ± 0.002	0.037 ± 0.002	0.036 ± 0.002
system B without GalCer ²³		0.08 ± 0.02	0.08 ± 0.02	0.07 ± 0.02
system C without GalCer ²³		0.5 ± 0.2	0.67 ± 0.06	0.8 ± 0.2

liquid-disordered like in system III, whereas system I is distinctly peaked in comparison. The GalCer–GalCer distribution is not shown because it is statistically not significant because of the small number of GalCer molecules in the simulated systems.

Whereas the scatter of the data in Figures 7 and 8 could be smaller, one can conclude that cholesterol molecules tend to organize among themselves and form local clusters with some internal structure. These structures are analyzed elsewhere in detail in a recent study (H. Martinez-Seara et al., unpublished). Furthermore, GalCer and PSM favor cholesterol and give rise to locally ordered structures, whereas the role of POPC is more passive.

3.6. Sugar Headgroup Orientations. To study further how hydrogen bonding with CHOL molecules affects GalCer headgroup orientation, we have investigated the directional vectors of the sugar headgroup for molecules with and without hydrogen bonds to CHOL molecules, as described above in Section 2.2. The angle distributions have been calculated between the bilayer

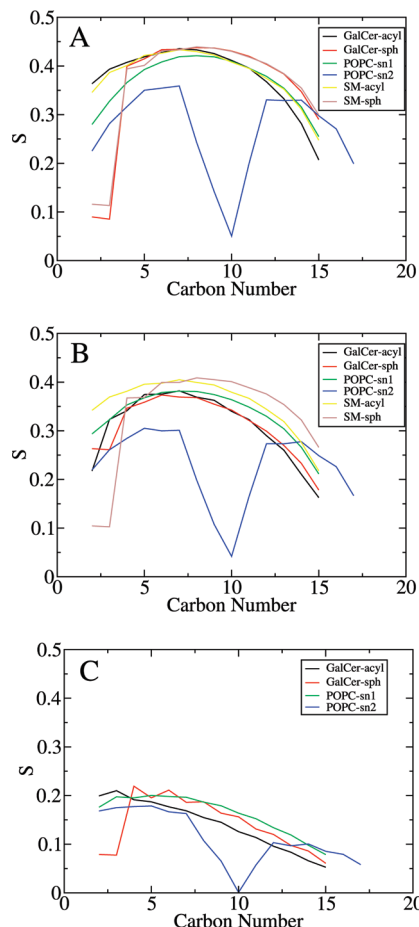


Figure 6. Order parameters (S_{CD}) for the different chains for each simulated system: (A) system I, (B) system II, and (C) system III. Small carbon numbers correspond to those close to the headgroup. Error bars are about the thickness of the line type used.

normal and two different vectors, as shown in Figure 2. The percentage of cholesterol-bonded GalCer molecules was found to be 23% for system I and 18% for system II.

Angle distributions for the headgroup vector, for systems I and II, are shown in Figure 9. One finds for both systems that when GalCer is bonded with CHOL, the sugar headgroup tilts considerably toward CHOL from the bilayer normal. In system I, the GalCer headgroup favors angles of 20 to 80° from the bilayer normal when it is not bonded to CHOL, whereas when bonded to CHOL, the favored angles are between 50 and 110°.

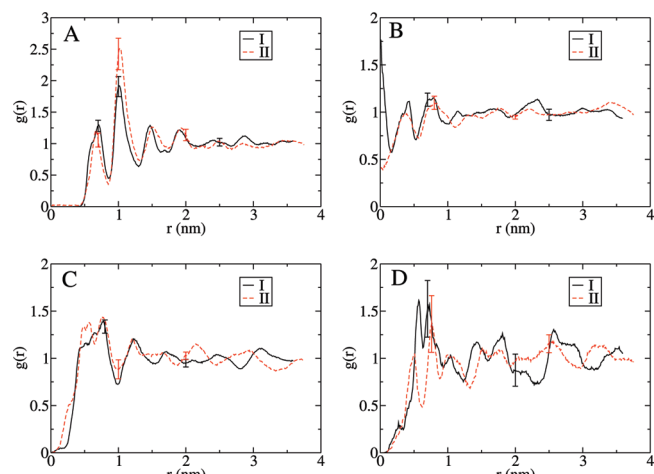


Figure 7. Radial distribution functions of different lipid components around CHOL molecules in systems I and II. (A) CHOL–CHOL pairs, (B) CHOL–POPC, (C) CHOL–PSM, and (D) CHOL–GalCer.

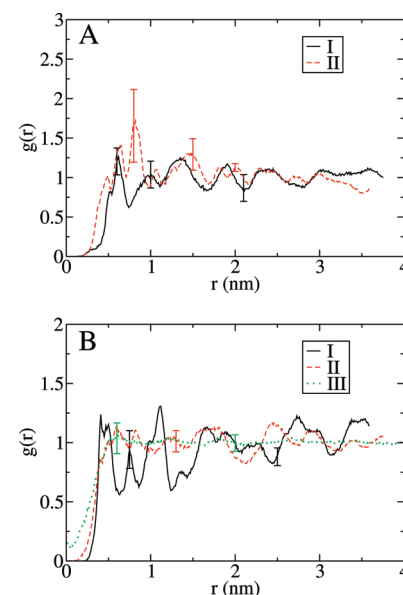


Figure 8. Radial distribution functions (RDFs), $g(r)$, of POPC and PSM molecules around GalCer molecules. (A) RDFs for GalCer–PSM pairs and for (B) GalCer–POPC pairs.

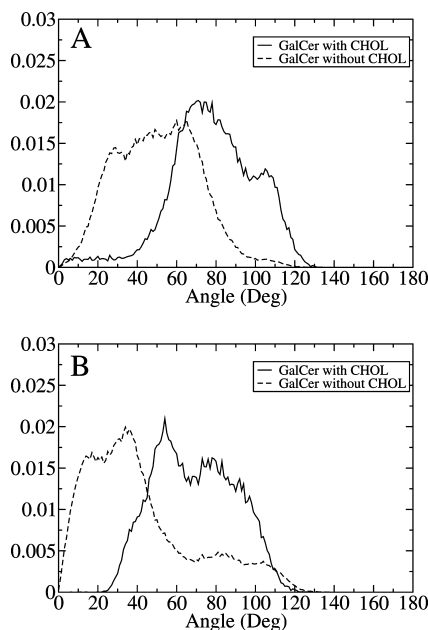


Figure 9. Distributions of GalCer headgroup orientations for GalCer molecules with and without hydrogen bonds to CHOL. The angle (α) is defined between the normal of the bilayer and the vector along the GalCer headgroup plane. (A) System I and (B) system II.

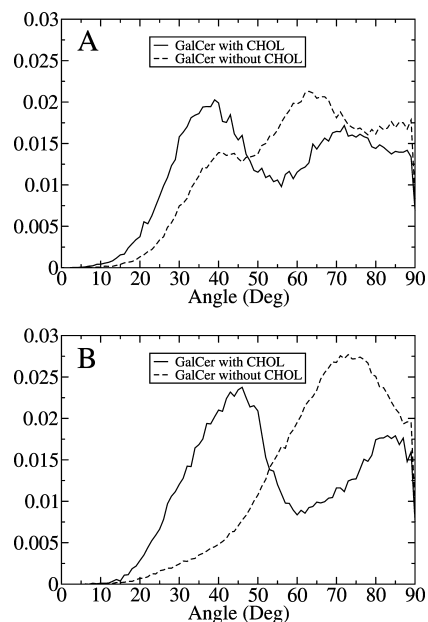


Figure 10. Distributions of GalCer headgroup orientations for GalCer molecules with and without hydrogen bonds to CHOL. The angle (β) is defined between the normal of the bilayer and the normal of the plane defined by the GalCer headgroup. (A) System I and (B) system II.

Similar to system II, the most favored angles are between 0 and 60° for GalCer without hydrogen bonds and between 30 and 110° for GalCer bonded to CHOL. For system II, the orientations of the GalCer molecules without hydrogen bonds to CHOL are distinctly more ideal than those for system I. This can also be clearly noticed in the distributions for the normal vector (Figure 10), with the GalCer molecules in system II without hydrogen bonds clearly favoring larger angles than those in system I.

The results highlight the role of sphingolipids in shielding cholesterol from the water phase: because of its hydrophobicity, cholesterol prefers to be shielded from water by the hydrated

TABLE 3: Average Number of Hydrogen Bonds from One Molecule of the First Type to Molecules of the Second Type^a

molecule pair	system		
	I	II	III
GalCer–POPC	2.1	3.1	5.0
GalCer–PSM	2.0	0.9	
GalCer–CHOL	0.3	0.3	
CHOL–POPC	0.60	0.69	
CHOL–PSM	0.17	0.12	
CHOL–GalCer	0.05	0.05	
PSM–POPC	0.37	0.50	
PSM–PSM	1.12	1.13	
PSM–GalCer	0.3	0.2	
PSM–CHOL	0.17	0.12	
POPC–PSM	0.36	0.24	
POPC–GalCer	0.3	0.3	0.2
POPC–CHOL	0.60	0.33	

^a Errors are <5%.

headgroup of GalCer. This “umbrella effect”⁴⁷ is one of the mechanisms that has been proposed for the selective, specific interaction between CHOL and sphingolipids. Our results picture its emergence for GalCer. A similar effect has been previously found for CHOL interacting with sphingomyelin.⁴⁸ Because glycerophospholipids seem to lack this property, or it is weaker compared with sphingolipids, it is apparently characteristic to the sphingosine backbone.

3.7. Hydrogen Bonding. The calculated average number of hydrogen bonds (H-bonds) per molecule with different molecular species is shown in Table 3. We focus here on cholesterol and its hydrogen bonding with the other lipid types, and thus we mainly consider systems I and II.

The presented data for CHOL indicate that in the four-component systems it forms more H-bonds with POPC than with PSM or GalCer. This observation is consistent with previous studies of two-component lipid bilayers,⁴⁸ although in binary systems the network of hydrogen bonding between CHOL and PSM is more extended and more dense than that between CHOL and POPC.^{49–52}

Considering GalCer, in system I, GalCer molecules are bonded to POPC and PSM in equal amounts, showing no preference between the two. In system II, GalCer prefers hydrogen bonding with POPC rather than PSM. In both cases, the H-bonds between GalCer and CHOL are rare compared with hydrogen bonding between GalCer and the phospholipids.

The above highlights H-bonding as such, with no reference to the relative number of molecules and donor/acceptor groups associated with hydrogen bonding. When this is taken into account, the picture changes inevitably: CHOL has just one hydroxyl group participating in hydrogen bonding, whereas both POPC and PSM have several donor/acceptor groups and GalCer has even more because of its sugar headgroups, allowing it to form approximately 4.5–5.0 hydrogen bonds per molecule (excluding those with water).

The relative numbers of GalCer and PSM molecules can also be taken into account by calculating the number of hydrogen bonds per possible molecule pair: CHOL has twice the number of hydrogen bonds with GalCer than PSM, although POPC still has the most bonds. A similar analysis for PSM shows that approximately the same number of hydrogen bonds are formed to GalCer and other PSM molecules, but the number of bonds to POPC molecules is significantly smaller.

A more detailed analysis of hydrogen bonding and charge pairs showed that the pattern of hydrogen bonds among CHOL,

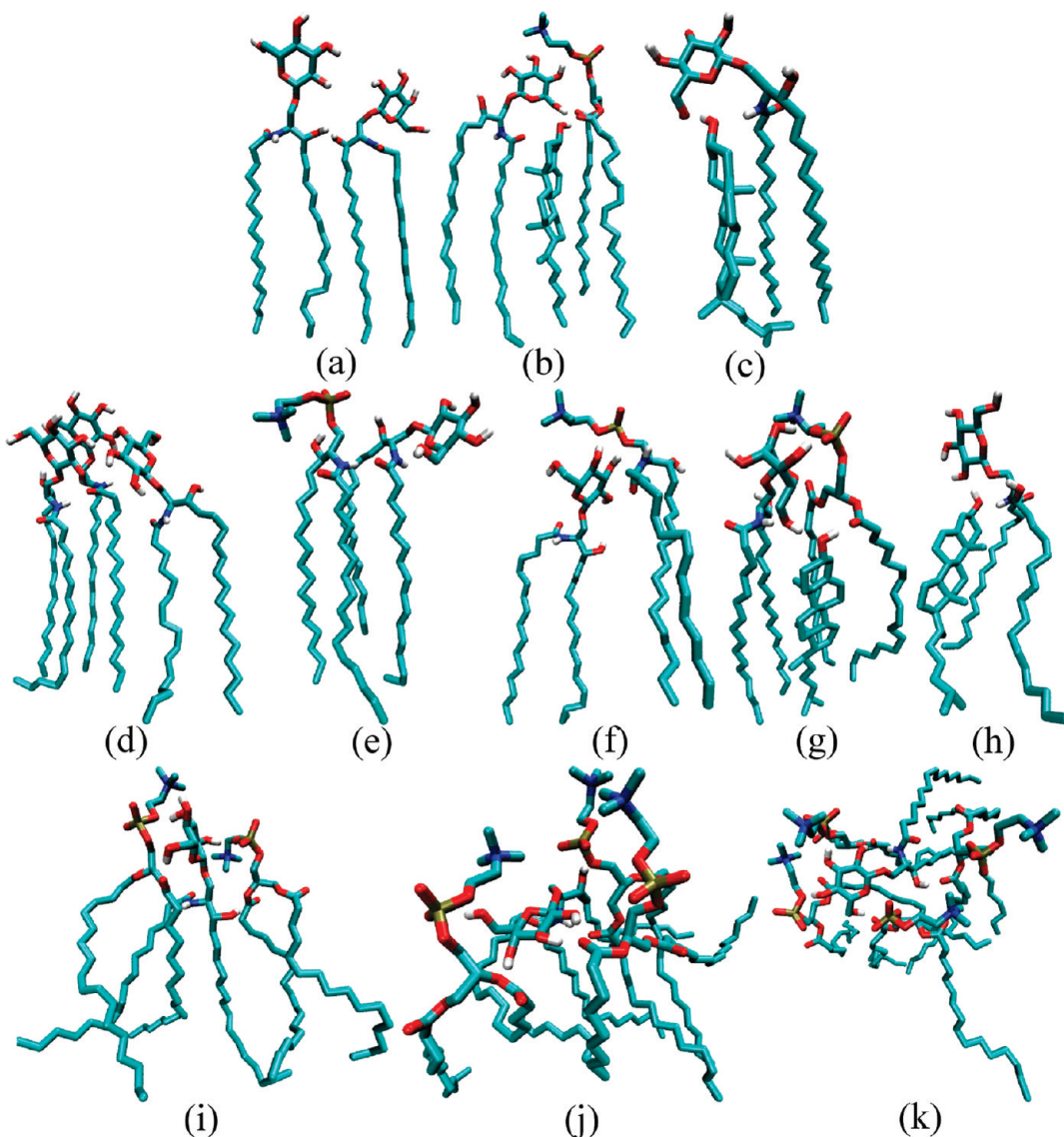


Figure 11. Molecules from the simulated systems. System I: plots A–C; system II: plots D–H; and system III: plots I–K. See Section 3.8 for descriptions of the molecular configurations.

POPC, and PSM is similar to that described in previous papers.^{23,48,53,54} For instance, for POPC, the main donor for hydrogen bonding is the carbonyl group of the *sn*-2 chain. The number of charge pairs formed between CHOL and POPC is 0.65 in system I and 0.38 in system II per CHOL molecule. Similar numbers for charge pairs between CHOL and PSM are 0.59 for system I and 0.42 for system II. Unlike the hydrogen bonds, the number of formed charge pairs does not indicate a clear preference for CHOL–PSM bonds, but rather both types seem equally probable.

3.8. Molecular Configurations. Snapshots of suggestive molecular configurations found in the simulations are shown in Figure 11. The first three subfigures (A–C) are taken from system I, the next five (D–H) are from system II, and the last three (I–K) are from system III.

Figure 11A shows two GalCer molecules interacting through a hydrogen bond between the hydroxyl groups. For GalCer molecules found in the simulations, this seemed to be a very typical interaction. Two different cases of GalCer interacting with CHOL are shown in Figure 11B,C. In the first one, the interaction is mediated by a POPC molecule bonded to GalCer through several hydrogen bonds, whereas

in the second case, the two are interacting directly. It can be seen that direct interaction with CHOL forces the GalCer headgroup to tilt considerably. The preference for mediated interactions is a possible explanation for why three-component systems of GalCer, PSM, and CHOL have been found to form ordered domains, whereas GalCer does not readily form cholesterol-enriched ordered domains without the presence of PSM.⁶

Figure 11D shows the stable cluster formed by three GalCer molecules is stuck to the other two through hydrogen bonds between the sugar headgroups. Surprisingly, the two face-to-face molecules are bonded primarily through hydrogen bonds between the functional groups of their stems and only indirectly through the headgroups. Another interaction of GalCer through the functional groups in the stem is seen in Figure 11E, this time with PSM. Figure 11F shows a case where several bonds are formed between a PSM molecule and the GalCer headgroup, pushing the PSM outward. This illustrates one way GalCer can increase the thickness of the lipid bilayer through interactions with PSM and POPC. Figure 11G,H shows additional examples of both mediated and direct interaction between GalCer and CHOL, this time from system II. Interestingly, the three-

molecule complex in Figure 11G is bound together through as many as seven hydrogen bonds.

Figure 11I–K shows how GalCer can form hydrogen bonds with multiple POPC molecules in the liquid-disordered phase (system III), first with two, then three, and finally four different molecules. Each of these complexes is bound by approximately six hydrogen bonds.

4. Concluding Remarks

Glycolipids are recognized as important lipid components in cellular membranes and in lipid rafts in particular, yet the molecular-scale interactions between glycosphingolipids and other raft components such as cholesterol and sphingomyelin are poorly understood. In this study, our objective has been to shed light on this issue using atomistic molecular dynamics simulations.

Whereas glycosphingolipids have only minor influence on membrane packing and ordering, their effect on membrane thickness and lateral diffusion has turned out to be substantial. These effects largely stem from the glycosphingolipids' preference for interdigitation, which is considerable despite the fact that the hydrocarbon chains in GalCer considered in this work (with palmitoyl side chain) are essentially of equal length. That is, interdigitation of GalCer does not arise from the asymmetry of lipid chain lengths but rather it is related to intermolecular interactions: we have found that the headgroup of GalCer resides at an essentially fixed position with respect to the POPC and CHOL molecules, slightly under the headgroup of POPC. This drives GalCer to find more room from the membrane center, promoting interdigitation. Furthermore, in addition to the slowing down of lateral diffusion, the interdigitation of GalCer likely also has a role to play in membrane viscosity between the two membrane leaflets, increasing the friction between the monolayers. The importance of interdigitation is highlighted by the fact that it has been found to change membrane morphology and affect domain formation for sphingosine-based lipids.⁵⁵ Interdigitation also, by definition, changes packing in the hydrophobic center of a membrane and hence alters the lateral pressure profile.⁵⁶ As has been demonstrated for raft-like systems, changes in lateral pressure may lead to a change in membrane protein activation.^{23,57} In summary, the observed interdigitation for GalCer is a genuinely interesting phenomenon, and its consequences will be considered in depth in future studies.

Meanwhile, because the lipid conformational order is not affected by GalCer, it seems apparent that the hydrophobic thickness of the bilayers does not change to a significant degree. Regarding membrane proteins and their hydrophobic thickness, this suggests that their solubility in rafts is driven more by cholesterol rather than glycosphingolipids. However, because some membrane proteins include sphingolipid binding motifs,⁵⁸ the role of glycosphingolipids is more extensive, not being related to membrane packing only.

A characteristic feature of GalCer is its tendency for a strong hydrogen bonding network with molecules in its vicinity. Of particular interest is the hydrogen bonding between GalCer and cholesterol. We have found these two molecules to prefer one another in the present four-component raft-like membrane system, which is highlighted in the shielding, or umbrella effect⁴⁷ of the glycosphingolipid with cholesterol: the sugar headgroup of GalCer covers CHOL, shielding its hydrophobic regions from contact with water. The effect observed here is, to our knowledge, the first time it has been reported for GalCer. The shielding effect and its biological importance in the context of

lipid rafts and glycolipids have been recently discussed by Lingwood and Simons⁵⁹ and noted as one of the possible mechanisms for cholesterol selectivity and sorting. Overall, the associative potential of GalCer with other raft components is evident because the hydrogen bonding of GalCer is strong overall. The role of PSM is also relevant because it hydrogen bonds mostly with GalCer and PSM, providing the third component of the favored interactions inside raft domains.

In summary, when glycosphingolipids are compared with sphingomyelin in a raft-like protein-free membrane, the role of glycosphingolipids is mostly clearly associated with cholesterol and the slowing down of lateral diffusion. The future challenges are many but mainly related to considerations of raft-like membranes with membrane proteins. For reasons mostly related to the computational cost of dealing with proteins in a many-component membrane system, raft-associated membrane proteins have not yet received the attention that they would deserve from the simulation and modeling community. There is reason to urge more research in this direction.

Acknowledgment. We thank the financial support by the Glycoscience Graduate School (AH), the Academy of Finland (A.H., T.R., I.V.), and the Natural Sciences and Engineering Research Council of Canada (M.K.). We also wish to thank the HorseShoe (DCSC) supercluster at the University of Southern Denmark and the Finnish IT Centre for Scientific Computing for computer resources.

References and Notes

- (1) Hakomori, S. *Glycoconjugate J.* **2004**, *21*, 125–137.
- (2) Pike, L. J. *Biochem. J.* **2004**, *387*, 281–292.
- (3) Simons, K.; Ikonen, E. *Nature* **1997**, *387*, 569–572.
- (4) Degroote, S.; Wolthoorn, J.; van Meer, G. *Semin. Cell Dev. Biol.* **2004**, *15*, 357–387.
- (5) Niemela, P.; Hyvonen, M. T.; Vattulainen, I. *Biochim. Biophys. Acta* **2009**, *1788*, 122–135.
- (6) Westerlund, B.; Slotte, J. P. *Biochim. Biophys. Acta* **2009**, *1788*, 194–201.
- (7) Ramstedt, B.; Slotte, J. P. *Biochim. Biophys. Acta* **2006**, *1758*, 1945–1956.
- (8) Eggeling, C.; Ringemann, C.; Medda, R.; Schwarzmann, G.; Sandhoff, K.; Polyakova, S.; Belov, V. N.; Hein, B.; von Middendorff, C.; Schonle, A.; Hell, S. W. *Nature* **2009**, *457*, 1159–1163.
- (9) Haas, N. S.; Shipley, G. G. *Biochim. Biophys. Acta* **1995**, *1240*, 133–141.
- (10) Christie, W. W. The Lipid Library, 2007. <http://www.lipidlibrary.co.uk>.
- (11) Maggio, B.; Fanani, M. L.; Rosetti, C. M.; Wilke, N. *Biochim. Biophys. Acta* **2006**, *1758*, 1922–1944.
- (12) Maunula, S.; Björkvist, Y. J. E.; Slotte, J. P.; Ramstedt, B. *Biochim. Biophys. Acta* **2007**, *1768*, 336–345.
- (13) Björkvist, Y. J. E.; Nyholm, T. K. M.; Slotte, J. P.; Ramstedt, B. *Bioophys. J.* **2005**, *88*, 4054–4063.
- (14) Lins, R. D.; Straatsma, T. P. *Biophys. J.* **2001**, *81*, 1037–1046.
- (15) Shroll, R. M.; Straatsma, T. P. *Biophys. J.* **2003**, *84*, 1765–1772.
- (16) Mondal, S.; Mukhopadhyay, C. *Langmuir* **2008**, *24*, 10298–10305.
- (17) Zaraiskaya, T.; Jeffrey, K. R. *Biophys. J.* **2005**, *88*, 4017–4031.
- (18) Rög, T.; Vattulainen, I.; Karttunen, M. *Cell. Mol. Biol. Lett.* **2005**, *10*, 625–630.
- (19) Rög, T.; Vattulainen, I.; Bunker, A.; Karttunen, M. *J. Phys. Chem. B* **2007**, *111*, 10146–10154.
- (20) Chong, T. T.; Hashim, R.; Bryce, R. A. *J. Phys. Chem. B* **2006**, *110*, 4978–4984.
- (21) Liu, P.; Izvekov, S.; Voth, G. A. *J. Phys. Chem. B* **2007**, *111*, 11566–11575.
- (22) Lopez, C. A.; Rzepiela, A. J.; de Vries, A.; Dijkhuizen, L.; Hunenberger, P. H.; Marrink, S. J. *J. Chem. Theory Comput.* **2009**, *5*, 3195–3210.
- (23) Niemelä, P.; Ollila, S.; Hyvonen, M. T.; Karttunen, M.; Vattulainen, I. *PLoS Comput. Biol.* **2007**, *3*, 304–312.
- (24) Apajalahti, T.; Niemela, P.; Govindan, P. N.; Miettinen, M. S.; Salonen, E.; Marrink, S. J.; Vattulainen, I. *Faraday Discuss.* **2009**, *144*, 411–430.
- (25) Risselada, H. J.; Marrink, S. J. *Proc. Natl. Acad. Sci. U.S.A.* **2008**, *105*, 17367–17372.

- (26) Pandit, S. A.; Vasudevan, S.; Chiu, S. W.; Mashl, R. J.; Jakobsson, E.; Scott, H. L. *Biophys. J.* **2004**, *87*, 1092–1100.
- (27) Martinez, J. M.; Martinez, L. *J. Comput. Chem.* **2003**, *24*, 819–825.
- (28) Bachar, M.; Brunelle, P.; Tielemans, D. P.; Rauk, A. *J. Phys. Chem. B* **2004**, *108*, 7170–7179.
- (29) Martinez-Seara, H.; Rög, T.; Karttunen, M.; Reigada, R.; Vattulainen, I. *J. Chem. Phys.* **2008**, *129*, 105103.
- (30) Martinez-Seara, H.; Rög, T.; Pasenkiewicz-Gierula, M.; Vattulainen, I.; Karttunen, M.; Reigada, R. *Biophys. J.* **2008**, *95*, 3295–3305.
- (31) Berendsen, H. J. C.; van der Spoel, D.; van Drunen, R. *Comput. Phys. Commun.* **1995**, *91*, 43–56.
- (32) Lindahl, E.; Hess, B.; van der Spoel, D. *J. Mol. Model.* **2001**, *7*, 306–317.
- (33) van der Spoel, D.; Lindahl, E.; Hess, B.; Groenhof, G.; Mark, A. E.; Berendsen, H. J. C. *J. Comput. Chem.* **2005**, *26*, 1701–1718.
- (34) Berendsen, H. J. C.; Postma, J. P. M.; van Gunsteren, W. F.; DiNola, A.; Haak, J. R. *J. Chem. Phys.* **1984**, *81*, 3684–3690.
- (35) Nose, S. *Mol. Phys.* **1984**, *52*, 255–268.
- (36) Hoover, W. *Phys. Rev. A* **1985**, *31*, 1695–1697.
- (37) Hess, B.; Bekker, H.; Berendsen, H. J. C. *J. Comput. Chem.* **1997**, *18*, 1463–1472.
- (38) Karttunen, M.; Roettler, J.; Vattulainen, I.; Sagui, C. In *Current Topics in Membranes: Computational Modeling of Membrane Bilayers*; Feller, S. E., Ed.; Elsevier: Amsterdam, 2008; pp 44–89.
- (39) Patra, M.; Hyvonen, M.; Falck, E.; Sabouri-Ghomi, M.; Vattulainen, I.; Karttunen, M. *Comput. Phys. Commun.* **2007**, *176*, 14–22.
- (40) Patra, M.; Karttunen, M.; Hyvonen, M. T.; Falck, E.; Lindqvist, P.; Vattulainen, I. *Biophys. J.* **2003**, *84*, 3636–3645.
- (41) Patra, M.; Karttunen, M.; Hyvonen, M. T.; Falck, E.; Vattulainen, I. *J. Phys. Chem. B* **2004**, *108*, 4485–4494.
- (42) Tielemans, D. P.; Berendsen, H. J. C. *J. Chem. Phys.* **1996**, *105*, 4871–4880.
- (43) Pasenkiewicz-Gierula, M.; Rög, T.; Kitamura, K.; Kusumi, A. *Biophys. J.* **2000**, *78*, 1376–1389.
- (44) Zhang, W.; Rög, T.; Gurtovenko, A. A.; Vattulainen, I.; Karttunen, M. *Biochimie* **2008**, *90*, 930–938.
- (45) Niemela, P.; Hyvonen, M. T.; Vattulainen, I. *Biophys. J.* **2006**, *90*, 851–863.
- (46) Niemelä, P. Computational Modelling of Lipid Bilayers with Sphingomyelin and Sterols. Ph.D. Thesis, Helsinki Institute of Physics, 2007.
- (47) Huang, J. Y.; Feigenson, G. W. *Biophys. J.* **1999**, *76*, 2142–2157.
- (48) Aitttoniemi, J.; Niemelä, P.; Hyvonen, M. T.; Karttunen, M.; Vattulainen, I. *Biophys. J.* **2007**, *92*, 1125–1137.
- (49) Rög, T.; Pasenkiewicz-Gierula, M. *Biophys. J.* **2006**, *91*, 3756–3767.
- (50) Zhang, Z.; Bhide, S. Y.; Berkowitz, M. L. *J. Phys. Chem. B* **2007**, *111*, 12888–12897.
- (51) Pandit, S. A.; Jakobsson, E.; Scott, H. L. *Biophys. J.* **2004**, *87*, 3312–3322.
- (52) Khelashvili, G. A.; Pandit, S. A.; Scott, H. L. *J. Chem. Phys.* **2005**, *123*, 34910.
- (53) Rög, T.; Vattulainen, I.; Pasenkiewicz-Gierula, M.; Karttunen, M. *Biophys. J.* **2007**, *92*, 3346–3357.
- (54) Rög, T.; Karttunen, M.; Vattulainen, I.; Jansen, M.; Ikonen, E. *J. Chem. Phys.* **2008**, *129*, 154508.
- (55) Pinto, S.; Silva, L.; de Almeida, R.; Prieto, M. *Biophys. J.* **2008**, *95*, 2867–2879.
- (56) Ollila, S.; Hyvönen, M. T.; Vattulainen, I. *J. Phys. Chem. B* **2007**, *111*, 3139–3150.
- (57) Ollila, S.; Rög, T.; Karttunen, M.; Vattulainen, I. *J. Struct. Biol.* **2007**, *161*, 311–323.
- (58) Fantini, J. *Cell. Mol. Life Sci.* **2003**, *60*, 1027–1032.
- (59) Lingwood, D.; Simons, K. *Science* **2010**, *327*, 46–50.

JP912175D